Published online 21 August 2023 *Nucleic Acids Research, 2023, Vol. 51, No. 17* ***9279–9293***
https://doi.org/10.1093/nar/gkad673

HELZ2: a new, interferon-regulated, human 3′-5′ exoribonuclease of the RNB family is expressed from a non-canonical initiation codon

Eric Huntzinger, Jordan Sinteff, Bastien Morlet and Bertrand Séraphin *

Institut de Génétique et de Biologie Moléculaire et cellulaire (IGBMC), Centre National de Recherche scientifique (CNRS) UMR 7104 - Institut National de santé et de Recherche Médicale (Inserm) U1258 - Université de Strasbourg, 1 rue Laurent Fries, Illkirch, France

Received March 21, 2023; Revised July 27, 2023; Editorial Decision July 28, 2023; Accepted August 10, 2023

ABSTRACT

Proteins containing a RNB domain, originally identified in *Escherichia coli* RNase II, are widely present throughout the tree of life. Many RNB proteins have 3′-5′ exoribonucleolytic activity but some have lost catalytic activity during evolution. Database searches identified a new RNB domain-containing protein in human: HELZ2. Analysis of genomic and expression data combined with evolutionary information suggested that the human HELZ2 protein is produced from an unforeseen non-canonical initiation codon in Hominidae. This unusual property was confirmed experimentally, extending the human protein by 247 residues. Human HELZ2 was further shown to be an active ribonuclease despite the substitution of a key residue in its catalytic center. HELZ2 RNase activity is lost in cells from some cancer patients as a result of somatic mutations. HELZ2 harbors also two RNA helicase domains and several zinc fingers and its expression is induced by interferon treatment. We demonstrate that HELZ2 is able to degrade structured RNAs through the coordinated ATP-dependent displacement of duplex RNA mediated by its RNA helicase domains and its 3′-5′ ribonucleolytic action. The expression characteristics and biochemical properties of HELZ2 support a role for this factor in response to viruses and/or mobile elements.

GRAPHICAL ABSTRACT

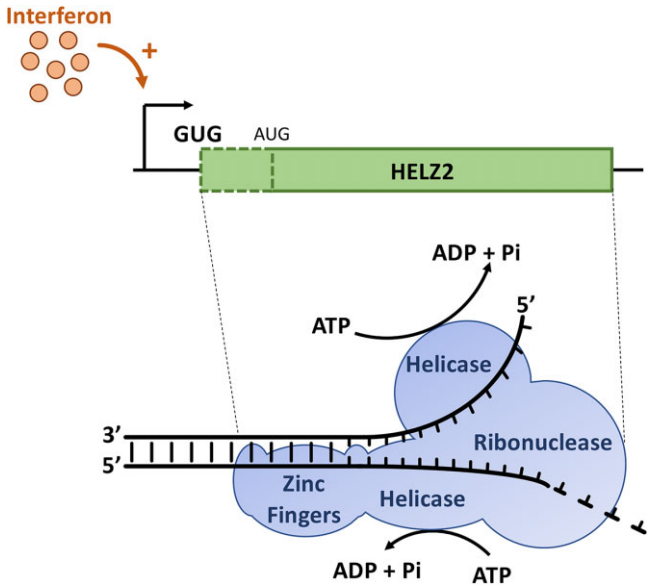

INTRODUCTION

During their life cycle, RNA molecules interact with numerous proteins that allow their synthesis, maturation, localization, translation and final degradation. Among the many factors interacting with RNA, ribonucleases play a unique role in participating both in the initial maturation of newly made RNAs and in their final degradation. Proteins belonging to numerous protein families are endowed with ribonuclease activity targeting cellular RNAs (1). Some of these factors are also mobilized by cells to defend themselves against pathogens such as RNA viruses, but may in some cases be diverted by the latter to facilitate their propagation.

One major ribonuclease family is defined by the presence of a RNB domain that catalyzes 3′- 5′ hydrolytic RNA

*To whom correspondence should be addressed. Tel: +33 3 88 65 33 36; Fax: +33 3 88 65 32 01; Email: seraphin@igbmc.fr
Present address: Jordan Sinteff. 77500 Chelles, France.

degradation. Founding members of this group, RNase II and RNase R were identified in *E. coli* (2). If closely related proteins are widely distributed in bacteria, distant family members are found in eukaryotes as well as in some archaea and viruses. In eukaryotes, a highly conserved RNB domain protein is the catalytic subunit of a decameric complex named the exosome that constitutes the major cellular 3′-5′ exonuclease in both the nucleus and the cytoplasm (3–7). If the exosome is conserved in the eukaryotic lineage, some RNB proteins are only present in specific clades of the eukaryotic tree. Hence, in human, three RNB domain-containing proteins have been characterized: DIS3 and DIS3L1 are exosome subunits (8,9), while DIS3L2 acts as an independent enzyme targeting uridylated RNAs (10–13). Whereas most proteins with a RNB domain are active nucleases, some have lost a catalytic activity during evolution but remain indirectly involved in RNA metabolism (14).

Database searches revealed the presence of another RNB domain-containing protein encoded by the human genome: HELZ2 (Helicase with Zinc Finger 2, also known as PDIP-1 or PRIC285). The presence of a RNB domain in HELZ2 has been overlooked in most studies involving this protein, possibly because of the emphasis given to its helicase and zinc finger domains in its HELZ2 acronym. Interestingly, however, expression of HELZ2 has been shown to be induced by interferon in mammalian cells (15), a property conserved in fish cells (16) as well as zebrafish embryo (17). In agreement, mimicking a viral infection by transfecting RNA or double-stranded DNA in mouse embryonic fibroblasts also induces HELZ2 mRNA expression (18). Analysis in chicken cells demonstrated that HELZ2 is controlled by the MDA5 receptor that senses double-stranded RNA (19). However, not all RNA viruses induce HELZ2 expression in every cell type, since infection of Saos-2 human osteosarcoma cells by Zika virus apparently has no effect (20). Consistent with the regulation of HELZ2 by interferon and pattern recognition receptors, a study reported that it mediates the inhibition of Dengue virus infection in human hepatic cells induced by IFN-α (21). In line with this observation, downregulation of HELZ2 expression reduces the antiviral effects of IFN-a against hepatitis C virus (HCV) infection (22). More recently, HELZ2 was found among the genes whose expression is upregulated in cells following SARS-CoV-2 infection (23,24). A CRISPR screen suggested further that HELZ2 may have a proviral action for SARS-CoV-2 (25). Beyond human systems, control of viruses by HELZ2 extends to birds as inhibition of HELZ2 facilitated infection by Duck Tembusu virus (26). Apart from viruses, HELZ2 was also reported to inhibit retrotransposition of human LINE1 (27). Links of HELZ2 with autoimmune diseases have also been identified by population genetics: an autoimmune disease locus in B cells and an autoimmune liver disease named primary biliary cholangitis are associated with variants at the HELZ2 locus (28,29). Also, HELZ2 somatic mutations were often found in cells from cancer patients. Finally, *Helz2*-knockout mice were shown to be resistant to high-fat diet-induced obesity, glucose intolerance, and hepatosteatosis (30). These phenotypes have been explained by central leptin resistance and by the increase in leptin receptor mRNA in the liver of the mutant mice, leading to a decrease in lipogenesis as well as an increase in fatty acid oxidation. To study the molecular contribution of HELZ2 to these processes, we decided to characterize the organization and activities of the human protein. Detailed analyses uncovered that human HELZ2 is longer than the sequence currently listed in databases as it is translated from a non- canonical start codon. Analysis of the full-length HELZ2 sequence revealed various domains including several copies of two types of Zn fingers and two helicase domains, in addition to the RNB domain. Biochemical analyses demonstrate that, despite the presence of a non-consensus residue at a critical position of its RNB active site, HELZ2 is an active 3′-5′ exonuclease, in agreement with data from a recent study (27). HELZ2 mutations found in cells from some cancer patients abolish this activity. We further show that the RNA helicase domains synergize with the RNB domain to allow degradation of structured RNA, a feature that may be important to target viruses or structured RNAs.

MATERIALS AND METHODS

Construction of eukaryotic expression vectors

The sequence encoding HELZ2β was amplified respectively from p3XFLAG-CMV7.1 HELZ2β (kind gift from Dr T. Tomaru), and inserted between the EcoRI-SalI sites of pEGFP-C1 vector (Clontech) giving pBS5528. For the cloning of the sequence encoding the N-terminal extension, a fragment of 897 nucleotides, covering the extension and the first 756 nucleotides of HELZ2β, overlapping the first exon, was amplified from genomic DNA and inserted into EcoRI-ClaI sites into peGFPC1-HELZ2β to give pBS6283. The sequence encoding human Dis3L1 was amplified from HEK293 cDNA preparation and then inserted between XhoI and SalI sites of pEGFP-C1 vector giving pBS6465. Subsequent modifications of these vectors were made by mutagenesis PCR. Original clones and derivatives were verified by Sanger sequencing.

For luciferases assays, complementary oligos containing the 5′UTR of HELZ2 mRNA and the 4 first codons of HelZ2β (nts 1 to 160) and the first 35 nts of firefly luciferase were annealed and extended by PCR. The resulting product was then digested and inserted between HindIII-KasI sites of pGL3 vector (Promega) giving pBS6288. Subsequent modifications of this vector were made by mutagenesis PCR. Original clones and derivatives were verified by Sanger sequencing. Oligonucleotides and plasmids used for this study are listed in Supplementary Tables S1 and S2 respectively.

Cell culture and transfections

HEK293 cells (ATCC CRL-1573) were maintained in DMEM medium containing 4.5 g/l glucose, GlutaMAX, 10% fetal calf serum and 40 μg/ml gentamicin. They were transfected with Lipofectamine^{2000} transfection reagent (ThermoFischer) according to the manufacturer's recommendation and processed 24–48 h post-transfection.

HeLa cells were maintained in DMEM medium containing 1 g/l glucose, 10% fetal calf serum and 40 μg/ml gentamicin. For interferon β stimulation, cells were seeded in

6 well plates and then mock-treated or treated with 5000 U/mL of human recombinant IFNβ (R&D systems, 8499-IF/CF) for 24 h.

Luciferase assay

HEK293 cells were seeded in 12-well plates and then co-transfected with 500 ng of firefly luciferase and 250 ng of renilla luciferase vectors. After 24 h, cells are washed with PBS1X and then lysed with 250 μl of 1× Passive Lysis Buffer (Promega). Firefly and renilla luminescences were then monitored with Dual-Glo Luciferase Assay kit (Promega) in a Berthold luminometer. Firefly values were normalized with renilla values to control for transfection efficiency.

Microscopy

HEK293 cells were grown on coverslips and transfected with pEGFPC1-HELZ2. After 48 hours, cells were fixed with 4% paraformaldehyde that was then neutralized by incubation with 0.125 M glycine followed by three washes with PBS 1×. Cells are then incubated for 30 s with DAPI diluted at 1/10 000. After three more washes, coverslips with cells were deposited on a glass slide together with one drop of mounting medium (ProLong Gold antifade reagent from Invitrogen). Microscopic images were taken with a Leica DM4000 B with an objective HC PL APO 100 × 1.40 oil CS2 and equipped with a Hamamatsu ORCA-Flash 4.0 LT C11440 camera.

Western blotting

Western blotting was performed using standard procedures and blots were visualized with Amersham Imager 600 or 800 (GE Healthcare). GFP fusion proteins were revealed with mouse monoclonal antibody anti-GFP (JL-8, Clontech) used at 1/2000 dilution. Anti-mouse IgG HRP-linked antibody (Cell Signaling Technology, 7076) was used as secondary antibody and revelation was performed with the Luminata Crescendo Western HRP Substrate (Millipore).

Oligonucleotides and RNA labeling

RNA and DNA oligonucleotides (100 pmol) were 5′ end-labeled using T4 PNK (ThermoFischer) and γ-P^{32} ATP according to manufacturer instructions. Reactions were stopped by addition of 5 μl of 0.25 M EDTA, supplemented with 2X RNA loading dye (ThermoFischer) and loaded on a 6% polyacrylamide-urea 8M gel for purification. After migration, bands corresponding to radiolabeled oligonucleotides were identified by autoradiography, excised and eluted overnight at 4°C in elution buffer (20 mM Tris–HCl pH 7.5, 0.25 M sodium acetate, 1 mM EDTA, 0.25% SDS). The next day, supernatants were recovered, phenol-chloroform extracted and precipitated. The resulting pellets were resuspended in 11 μl of ddH2O. RNA and DNA oligonucleotides used for the assays are listed in Supplementary Table S3.

Production of RNA-RNA duplexes

5′ end-labeled RNA was incubated with a 3-fold excess of complementary cold RNA in annealing buffer (60 mM KCl, 6 mM HEPES pH 7,5, 0,2 mM $MgCl_2$). After 2 min incubation at 90°C, the mixture was allowed to cool slowly to room temperature. Samples were then loaded on a 6% native polyacrylamide gel in 1× TBE and fractionated by electrophoresis. After migration, an autoradiography was performed to locate bands of interest and those were cut and eluted overnight at 4°C in elution buffer (20 mM Tris–HCl pH 7.5, 0.25 M sodium acetate, 1 mM EDTA, 0.25% SDS). The next day, supernatants were recovered, phenol–chloroform extracted, and precipitated. The resulting pellets were resuspended in 11 μl of ddH2O.

GFP-tagged protein immunoprecipitation for biochemical assay

Immunoprecipitation experiments were performed using GFP-Trap paramagnetic beads (Chromotek) as recommended by the manufacturer. Specifically, 48 hours after transfection cells grown in 15 cm diameter dishes were lysed for 20 min on ice in 500 μl lysis buffer (10 mM Tris–HCl pH 8.0, 150 mM NaCl, 0.5% Igepal CA-630, 1 mM DTT) supplemented with protease inhibitors (1× Complete Protease Inhibitor Cocktail EDTA-free, Roche). After centrifugation at 20 000 g for 20 min at 4°C, supernatants were recovered and protein concentrations were determined with Protein Assay Dye Reagent Concentrate (Bio-Rad). Per assay, 1 mg of cell lysates were then incubated with 5 μl GFP-Trap paramagnetic beads for 1 h at 4 °C mixing by rotation. After recovery, beads were washed three times with 1 ml wash buffer (10 mM Tris–HCl pH 8.0, 500 mM NaCl, 0.5% Igepal CA-630, 1 mM DTT). During the last wash, 10% of the beads were recovered for western blot analysis. The rest of the beads were aliquoted in separated tubes and resuspended in 45 μl of reaction buffer (10 mM Tris–HCl pH 8, 150 mM NaCl, 5 mM $MgCl_2$ and 1 mM DTT) and kept on ice until further use. Because of the limited yield preventing accurate determination of protein concentration, subsequent activity assays were performed with the tagged protein still bound to the beads (i.e. without elution).

RNase assay

To proteins bound to GFP-Trap beads (see above), 5 μl of a mix containing radiolabeled RNA and radiolabeled DNA diluted in reaction buffer (10 mM Tris–HCl pH 8, 150 mM NaCl, 5 mM $MgCl_2$ and 1 mM DTT) were added. Aliquots of 5 μl were taken at different time points and mixed with 1 μl of stop reaction buffer (1% SDS, 0.1 M EDTA) and 6 μl of 2× RNA loading dye (ThermoFischer). Samples were then incubated for 2 min at 90°C and then one-third was loaded on a 20% polyacrylamide-urea 8 M gel for separation. After the migration, gels were exposed to an imaging plate (Fuji) for 6 h and then revealed using a Typhoon FLA-9500. Bands were quantified using ImageQuant (Cytiva).

ATPase assay

To proteins bound to GFP-Trap beads (see above), 5 μl of a mix containing reaction buffer, α-P^{32} ATP (25 pmol) were

added. DNA (100 pmol) or RNA (100 pmol) were included as indicated. Aliquots of 10 μl were taken from reactions after 2 h and mixed with 1 μl of stop reaction buffer (1% SDS, 0,1 M EDTA). One microliter of each sample was then loaded on a thin-layer chromatography plate (PEI cellulose F, Merck) and resolved with KH_2PO_4 0.75 M buffer. In parallel, ATP and ADP were loaded as migration controls. ADP was produced by incubating radioactive ATP with cold ADP and nucleotide di-phosphate kinase (NDK, N2635-100UN, Sigma-Aldrich) for 30 min at 25°C. After the migration, dried TLC plates were exposed to an imaging plate (Fuji) for 2 hours and then revealed using a Typhoon FLA-9500. Signals were quantified using ImageQuant (Cytiva).

Assays with guanabenz acetate

RNase and ATPase assays were performed as described in the presence or absence of guanabenz acetate (sc-203590, Santa Cruz).

Sample preparation for mass spectrometry analyses

After 24 h of stimulation with interferon or mock treatment, cells were recovered and then lysed in RIPA buffer (50 mM Tris–HCl pH 7.4, 150 mM NaCl, 1% Igepal, 0.5% sodium deoxycholate, 0.1% SDS). Bradford assay was used to determine protein concentrations and equal amounts of extracts were further analyzed by mass spectrometry. The protein mixtures were precipitated with TCA 20% overnight at 4°C and centrifuged at 14 000 rpm for 10 min at 4°C. Protein pellets were washed twice with 1 mL of cold acetone and air dried. The protein extracts were solubilized in urea 2 M, reduced with 5 mM TCEP for 30 min and alkylated with 10 mM iodoacetamide for 30 min in the dark. Enzymatic digestion was performed at 37°C and overnight with 500 ng trypsin (Promega). Peptide mixtures were then desalted on C18 spin column and dried in a Speed-Vacuum.

LC–MS/MS analysis

Samples were analyzed using an Ultimate 3000 nano-RSLC coupled in line, via the NanoFlex- electrospray ionization source, with the Orbitrap Exploris 480 mass-spectrometer (Thermo Fisher Scientific) equipped with a FAIMS (high Field Asymmetric Ion Mobility Spectrometry) module. Peptide mixtures were injected in 0.1% TFA on a C18 Acclaim PepMap100 trap- column (75 μm ID × 2 cm, 3 μm, 100Å, Thermo Fisher Scientific) for 3 min at 6 μl/min with 2% ACN, 0.1% FA in H_2O and then separated on a BioZen peptide XB-C18 nano-column (75 μm ID × 25 cm, 2.6 μm, Phenomenex) at 350 nl/min and 45°C with a 60 min linear gradient from 9% to 30% buffer B (A: 0.1% FA in H_2O/B: 80% ACN, 0.1% FA in H_2O), regeneration at 9% B. Spray voltage were set to 2.1 kV and heated capillary temperature at 280°C.

The Orbitrap Exploris 480 was associated with the FAIMS module, set to −45 V as compensation voltage (CV). A cycle time of 1.2 s was chosen. For the full MS1 in DDA mode, the resolution was set to 120 000 at m/z 200 and with a mass range set to 330–1200. The full MS AGC target was 300% with a Max IT set to 100 ms. For the fragment spectra in MS2, AGC target value was 100% (Standard) with a resolution of 30 000 and the maximum Injection Time set to Auto mode. The intensity threshold was set at 5E3. Isolation width was set at 2 m/z and normalized collision energy was set at 30%. All spectra were acquired in centroid mode using positive polarity. Default settings were used for FAIMS with voltage applied as described previously, and with a total carrier gas flow set to 4.2 l/min.

Mass spectrometry data analysis

Proteins were identified by database searching using SequestHT (Thermo Fisher Scientific) with Proteome Discoverer 2.5 software (PD2.5, Thermo Fisher Scientific) on human FASTA database downloaded from UniProt (reviewed, release 2022_10_27, 20607 entries, https://www.uniprot.org/). Precursor and fragment mass tolerances were set at 7 ppm and 0.02 Da respectively, and up to 2 missed cleavages were allowed. For all the data, oxidation (M, +15.995 Da) was set as variable modification, and Carbamidomethylation (C, + 57.021 Da) as fixed modification. Peptides and proteins were filtered with a false discovery rate (FDR) at 1%. Label-free quantification was based on the extracted ion chromatography intensity of the peptides and realized with Perseus 1.6.15.0 (Max Planck Institute of Biochemistry). Biological triplicates were analyzed. The measured extracted ion chromatogram (XIC) intensities were normalized based on median intensities of the entire dataset to correct minor loading differences. For statistical tests, not detectable intensity values were treated with an imputation method, where the missing values were replaced by random values similar to the 10% of the lowest intensity values present in the entire dataset. Unpaired two-tailed *t*-tests, assuming equal variance, were performed on obtained $\log_2$ XIC intensities.

RESULTS

Human HELZ2 protein translation initiates with a non-canonical start codon

HELZ2 (also named PRIC285 or PDIP1) was initially identified by two independent groups in experiments aiming to identify novel partners for the DNA binding domains of PPARα and PPARγ (Peroxisomal Proliferator-Activated Receptor alpha and gamma) (31,32). A first isoform, named HELZ2α and corresponding to a protein of 231kDa, was identified by cDNA sequencing in the original study (31) (Figure 1A). The second study predicted a larger, N-terminally extended, isoform of 295kDa termed HELZ2β (32) (Figure 1A). While the two isoforms could be encoded by alternatively spliced mRNAs, 5′ RACE experiments performed by the second group failed to amplify the 5′ end of the cDNA encoding the α isoform suggesting that it was at best of low abundance (32). This conclusion is further supported by the results of RNase protection assays performed by the second team (32) and the mapping of transcription initiation sites that failed to confirm the start site of the HELZ2α mRNA (33). Moreover, a single mRNA corresponding in size to the one encoding the β isoform,

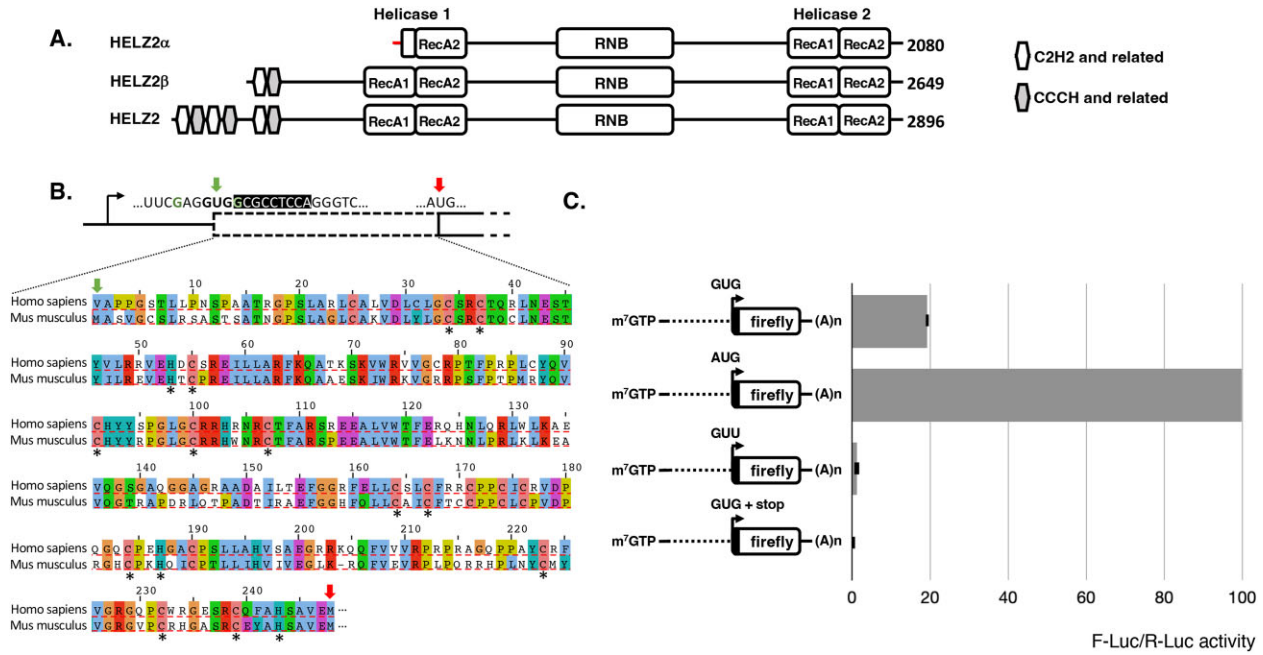

Figure 1. Human HELZ2 translation is initiated by a non-canonical initiation codon. (**A**) Domain organization of human HELZ2 and its previously described isoforms. The alternative sequence present at the N-terminus of the putative HELZ2α isoform that truncate the RecA1 domain of Helicase 1 is indicated in red. (**B**) Close-up view of human HELZ2 mRNA 5′ end organisation and sequence alignment of the N-terminal region of mouse HELZ2 (UniProt: E9QAM5) and the *in silico* translated sequence of human HELZ2 N-terminal extension. Top: black arrow: transcription start site of human HELZ2 mRNA. Continuous line: 5′UTR. Dashed box: human HELZ2 N-terminal extension. Above are indicated the non- canonical GUG initiation codon (green arrow) and the canonical initiation codon of HELZ2β (red arrow). The context surrounding the GUG codon is provided with nucleotides favorable for translation initiation at the non-canonical initiation codon shown in green. Nucleotides following the GUG codon with black background are included in the reporters used in Panel C. Below the schematic organization, an alignment of the N-terminal region of mouse HELZ2 and the *in silico* translated sequence of human HELZ2 N-terminal extension from the amino acid encoded by the GUG codon to the previously described initiating methionine of the HELZ2β isoform is shown. Note that in the absence of experimental data it is unclear whether the GUG start codon is decoded as M, V or both. The sequence alignment is colored for amino acid conservation using Clustal W and asterisks placed below the sequence indicate C and H residues of the conserved additional Zn fingers motifs. (**C**) Luciferase assay to evaluate HELZ2 translation initiation. Schemes of the reporters used are shown on the left. Dashed line: HELZ2 5′UTR. Black arrow: initiation codon or mutant thereof. Black box: nine nucleotides from HELZ2 sequence following the initiating codon. Open box: luciferase coding sequence. On the right: firefly luciferase activity normalized to co-transfected renilla luciferase for each construct.

and significantly longer than the one predicted to encode HELZ2α, was detected in Northern blots by the first group. Further, the predicted mRNA encoding HELZ2α contains an upstream out-of-frame AUG codon and a predicted 3′ splice site (31). Altogether, our synthesis of available data retrospectively supports the existence of a single mRNA with the α isoform probably not being relevant but rather derived from an incompletely spliced pre-mRNA.

Intriguingly, we noticed that the full-length cDNA contains a long 5′UTR of 893 bases (Figure 1B) that contains four out-of-frame AUG codons (Supplementary Figure S1). Moreover, the predicted human β isoform protein is significantly shorter than orthologs in many other mammals. For example, the predicted HELZ2 protein in mouse is about 300 amino acids longer than the human (2947 versus 2649 residues), with the main difference resulting from the absence in the human polypeptide of sequence similar to the N-terminal 247 residues of its mouse counterpart. Comparison of the mouse N-terminal extension with sequences encoded by the human genome indicates that a very similar sequence (65% identity) is encoded in frame and upstream of the β isoform AUG codon (Figure 1B). This, together with the presence of a GUG codon at position 152 in the human cDNA aligning with the mouse AUG codon, suggested that HELZ2 translation in human could initiate from a non-canonical start codon. The presence of a favorable context for translation initiation (a purine at position -3 and guanosine at position + 4 (34)) around the GUG codon further supported this hypothesis (Figure 1B). However, we could not rule out the possibility that human HELZ2 translation could initiate at another non- canonical codon such as CUG at cDNA position 140, which is also in a favorable context. Analysis of published ribosome profiling data supported the translation of the sequence upstream of the β isoform initiation codon (35) (Supplementary Figure S2). Moreover, the conservation of the unusual organization of the HELZ2 coding sequence, including the GUG codon present at position 152 in the human cDNA, in all Hominidae species argued that it is biologically relevant.

To validate the capacity of the 5′ extremity of the human HELZ2 mRNA to promote translation initiation at a non-canonical codon, we constructed a reporter in which the sequence starting at the HELZ2 mRNA transcription initiation site, extending to the GUG and including the following nine nucleotides were fused upstream of, and in-frame with, the coding sequence of firefly luciferase. As reference, we used the same construct in which the GUG codon has been substituted by an AUG codon. HEK293 cells were

transfected with the resulting plasmids together with a plasmid expressing renilla luciferase to normalize transfection efficiencies. Results indicate the GUG construct produced a significant level of luciferase, about 20% the level of an AUG codon in the same context (Figure 1C). To ascertain that the signal observed is due to translation at the GUG codon, and not to any downstream initiation event, two additional reporters were constructed. In the first one, the GUG codon at position 152 was mutated into a GUU, and in the second one, a stop codon was introduced 3 residues after the GUG codon (Figure 1C). The GUU construct produced only traces of luciferase about 20-fold less than the GUG construct, possibly products of inefficient translation initiation at other sites (e.g. CUG at position 140). Introducing a stop four codons downstream of the GUG codon reduced firefly luciferase levels to background (roughly 250-fold reduction compared to the GUG construct) indicating that translation initiates exclusively from the GUG of the HELZ2 sequence when present. Altogether, these results indicate that the GUG codon at position 152 can be used for translation initiation. We subsequently refer to the isoform initiated at this site as 'full-length HELZ2' and to the sequence present in full-length HELZ2 but absent from HELZ2β as 'extension'.

To establish whether HELZ2 translation initiates *in vivo* from the GUG codon at position 152, we performed mass spectrometry experiments. Interferon-responsive HeLa cells were used for tandem mass spectrometry analyses using as reference the human proteome present in the UniProt database completed by the sequence of the predicted extension. Biological triplicates of HeLa cells with and without interferon treatment were tested. Neither the HELZ2β nor the extension sequences were detected in cells growing in the absence of interferon. As expected, interferon treatment induced expression of many proteins (Figure 2A), including HELZ2. More importantly, peptides belonging to both the HELZ2β and the extension sequences were reproducibly detected after interferon stimulation (Figure 2A). This result indicates that translation initiates *in vivo* upstream of the AUG codon currently annotated as the start of the β isoform. Interestingly, the relative numbers of Peptide Spectrum Match (PSM, a first approximation of peptide abundance) for the extension and β isoform sequences were nearly proportional to the corresponding protein length (Figure 2B), suggesting that they were expressed at a similar level. While this is only indicative, it suggests that *in vivo* full-length HELZ2 is the main translation product.

Our observation of the existence of an extended 'full-length' isoform of HELZ2 raised the question of its intracellular localization. Indeed, the putative HELZ2α isoform was originally categorized as a nuclear protein colocalizing with PPARα (31) but more recent data suggest that HELZ2β may function in the cytoplasm to fulfill some of its functions (27). To address this issue, we used microscopy analyses to test the localization of transiently expressed full-length HELZ2 N-terminally tagged with GFP. Our results indicate that the full-length protein is well expressed and predominantly cytoplasmic with an overall diffuse distribution. In some cells, we noticed the presence of few bright foci that were probably enriched in GFP-HELZ2 (Figure 2C).

Altogether, our data indicate that HELZ2 protein expression is interferon-induced and that the use of a non-canonical translation initiation codon generates a hitherto unrecognized 'full- length' protein that localizes in the cytoplasm.

Domain organization of human HELZ2

Database searches and multiple sequence alignments reveal that human HELZ2 has a modular structure (Figure 1A). Full-length human HELZ2 contains six Zn finger or Zn finger-like domains at its N-terminus. These appear to be of both C2H2 and CCCH types. Some Zn fingers depart from the corresponding consensus but their characteristics, the alternating positioning of the two types, and the conservation of this arrangement in related proteins support these assignments (Supplementary Figure S3). The 1st, 3rd and 5th Zn fingers are distantly related to C2H2 domains that have been found in a number of proteins involved in RNA metabolism (36,37). Some of them were proposed to mediate interaction with double-stranded RNA. The alternating Zn fingers are of the CCCH family known to bind single-stranded RNA in a sequence-specific manner (38). This organization, including the presence of deviant members and additional conserved C and H amino acids suggests that the Zn fingers may cooperate to recognize complex RNA motifs. Alternatively, they could act independently, allowing HELZ2 to recognize different RNA partners in a combinatorial manner. Interestingly, four of these Zn fingers are encoded by the previously unnoticed N-terminal region of the human protein (Figure 1B). Their conservation in other animals supports further the translation of this region.

The N-terminal Zn finger region is followed by a RNA helicase domain, the RNB domain and a second helicase domain (Figure 1A, Supplementary Figure S4). Both helicase domains belong to the Upf1-like subgroup of the SF1 helicase superfamily. The 11 proteins of this subfamily mostly interact with RNA and are monomeric SF1-B 5′–3′ helicases (39). In between the two helicase domains, lies the RNB domain that, like for most proteins harboring this signature, is preceded by two cold-shock domains (CSD). The latters have been shown to guide the incoming substrate to the exoribonucleolytic catalytic site (Supplementary Figure S4). Most RNB domains are followed by a S1 domain. This domain, originally identified in *E. coli* ribosomal protein S1, is topologically related to CSD and also interacts with single-stranded RNA. Accordingly, the sequence of HELZ2, and the corresponding 3D-structure predicted by AlphaFold (40), suggest the presence of a structure with some characteristics of S1 domains downstream of the RNB domain of HELZ2 (Supplementary Figure S4).

The HELZ2 RNB domain exhibits ribonuclease activity *in vitro*

The HELZ2 RNB domain is unusual as the second of the four highly conserved aspartic acids thought to be catalytic in proteins containing an RNB domain (2,3,41) is replaced with an asparagine (Figure 3A). Interestingly, the canonical aspartate is found in HELZ2 sequences from monotremes and other vertebrates (Supplementary Figure S4). This observation questions whether the RNB domain of human

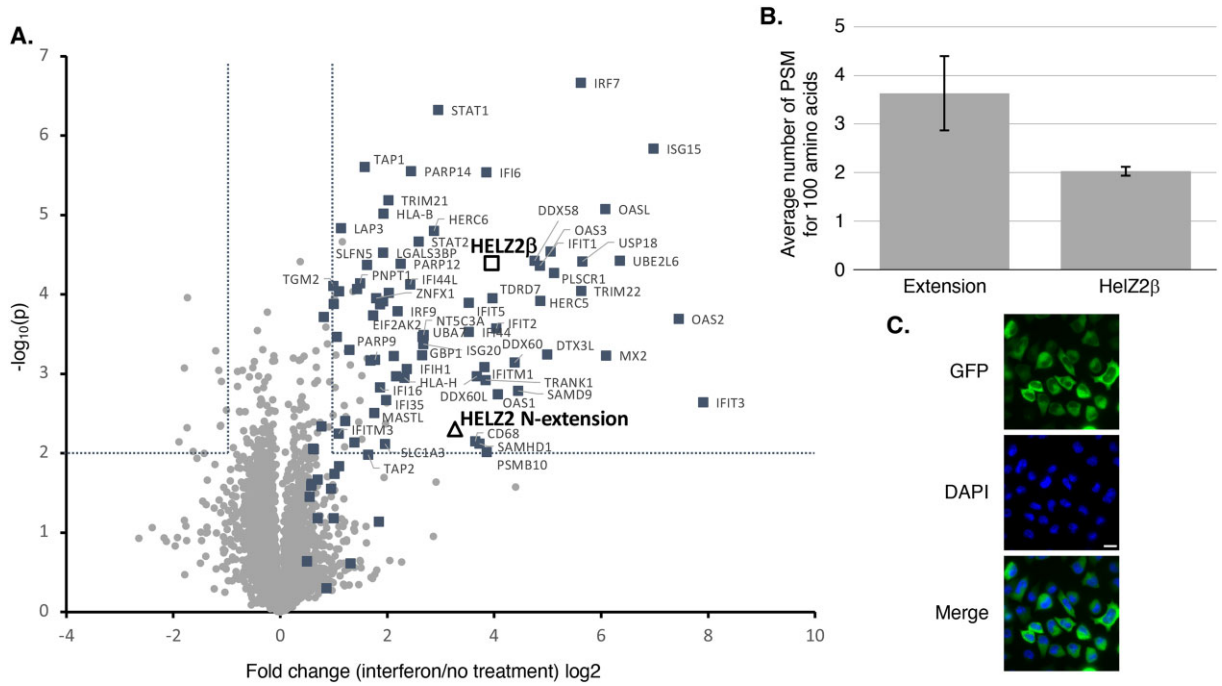

Figure 2. Mass spectrometry analysis of protein extracts from mock- or IFNβ- treated HeLa cells. (**A**) Volcano-plot showing the log2 fold change versus -$\log_{10}$(*P*-value) between mock- or interferon-treated HeLa cells. Analyses were performed in triplicate and a total of 4828 proteins were quantified by mass spectrometry. Filled or open squares indicate human proteins whose expression at mRNA or protein levels have been reported to be induced at least 3 fold by interferon in the Interferome Database (67). The names of some of these factors are indicated. Open square and triangle represent measurement for peptides corresponding to the HELZ2β isoform and the HELZ2 extension, respectively. All other proteins are indicated by grey dots. Dashed lines delimit regions of p-value higher or lower than 0.01 and up- or down-regulation of at least 2-fold. (**B**) Graphical representation of the number of PSM per 100 amino acids for the N-terminal extension sequence of HELZ2 and the HELZ2β isoform. (**C**) Representative microscopic image of HeLa cells transfected with a plasmid expressing GFP-HELZ2 to monitor its localization. Green: GFP signals, blue: DAPI signal, and merged. White scale bar: 15 μm.

HELZ2 lost its catalytic activity during mammalian evolution. To test whether human HELZ2 has nuclease activity we turned to *in vitro* assays. As our attempts to produce recombinant protein in bacteria or in baculovirus were unsuccessful, we used HEK293 cells transfected with plasmids encoding GFP-HELZ2 or GFP-HELZ2β for our biochemical tests. As a negative control, we used GFP-MBP. We also constructed derivatives of GFP-HELZ2 and GFP-HELZ2β, namely GFP-HELZ2 rnb$^-$ and GFP-HELZ2β rnb$^-$, carrying a D to N substitution at the third of the four conserved aspartate residues (Figure 3A) corresponding to position 1601 of full-length HELZ2 (1354 for HELZ2β) as this essential catalytic residue has been shown to coordinate magnesium (41) and its mutation in other RNB family members abolishes nuclease activity (2,3). (Note that this residue differs from the one naturally substituted by an asparagine in human HELZ2, Figure 3A.) Proteins were immunoprecipitated from extracts with GFP-Trap beads which were extensively washed before addition of a 5′ radiolabeled 35 nucleotide long synthetic DNA oligonucleotide and a 20 nucleotide long synthetic RNA oligonucleotide in a magnesium-containing buffer. The reaction was incubated at 37°C with regular shaking and aliquots were collected at different time points. In parallel, protein samples were collected to analyze the material present in the input and on the beads by western blot (Figure 3B). We observed that the GFP-MBP, GFP-HELZ2, GFP- HELZ2β wild types or mutants are all produced and immunoprecipitated in similar quantities allowing assessment of their nuclease activities (Figure 3B). We did not observe any changes in the intensity of the 35 nucleotides DNA band at all incubation times, regardless of the protein used (Figure 3C). This indicates that the HELZ2 protein and its derivatives do not have deoxyribonuclease activity. Analysis of the fate of the RNA oligonucleotide incubated in the presence of GFP-MBP reveals only background degradation after 1 h of incubation possibly owing to traces of contaminants (Figure 3C). In contrast, in the presence of either HELZ2 or HELZ2β, a strong decrease in the signal corresponding to the 20 nucleotides RNA was observed even at the earliest time points (only two minutes of incubation) (Figure 3C, D). Concomitantly with the disappearance of the full-length RNA substrate, we observe the appearance of degradation intermediates of progressively decreasing size during the time course experiment. These observations are consistent with the exonucleolytic 3′ to 5′ degradation of the RNA catalyzed by RNB domain-containing proteins. A final product of 4–5 nucleotides starts to accumulate after 8 minutes and is predominant at the two latest time points. Importantly, the observed nuclease activity is lost when proteins harboring the point mutation in the catalytic domain were used (*rnb$^-$*, Figure 3C, D). We compared the distribution and size of the degradation products with the one generated by another

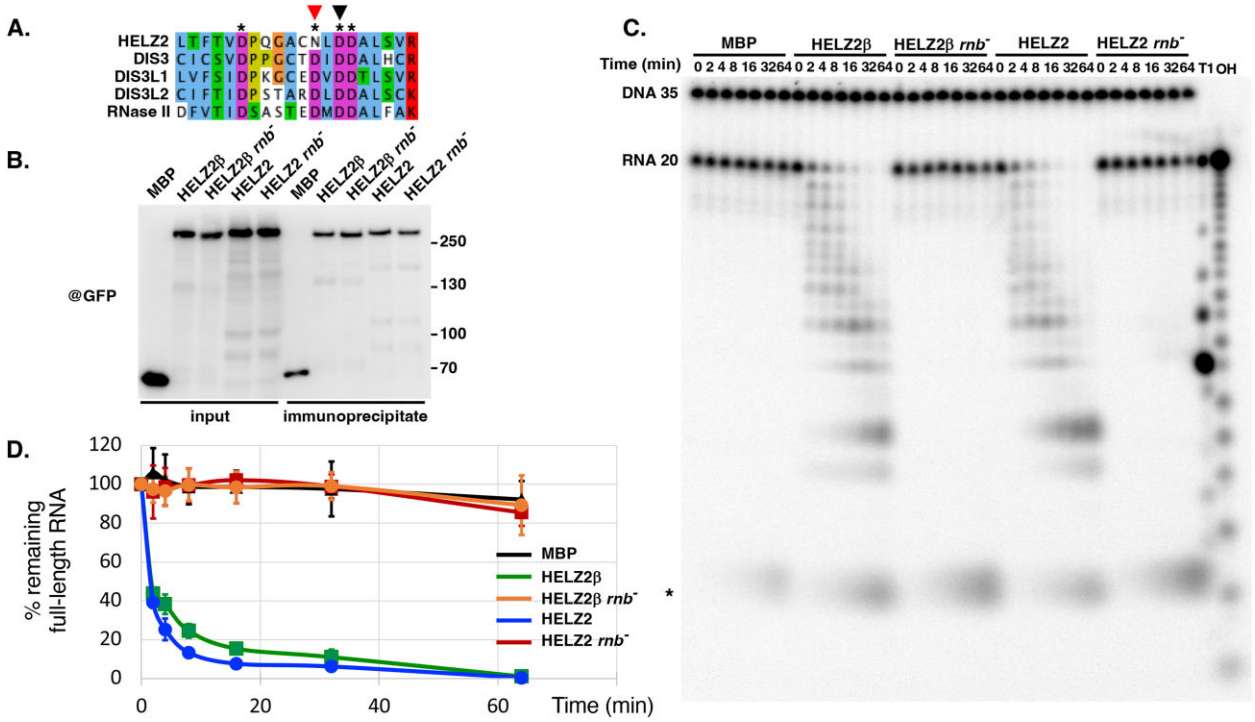

Figure 3. HELZ2 and HELZ2β are active ribonucleases. (**A**) Sequence alignment of the RNB domain catalytic region from human HELZ2 (Q9BYK8), DIS3 (Q9Y2L1), DIS3L1 (Q8TF46), DIS3L2 (Q8IYB7) and from bacterial RNaseII (P30850). Previously proposed catalytic residues are indicated by asterisks. The sequence alignment is coloured for amino acid conservation using Clustal W. The position naturally substituted by an asparagine in human HELZ2 is indicated by a red arrowhead while the aspartate mutated to an asparagine to inactivate the HELZ2 RNB domain (rnb$^-$) is indicated by a black arrowhead. (**B**) Western-blot using anti-GFP showing expression levels and immunoprecipitation efficiencies for the proteins used in the ribonuclease activity test. (**C**) Representative RNA degradation assay gel. Samples from the ribonuclease activity test were fractionated on a 20% polyacrylamide-urea gel. Numbers above the lanes represent incubation times in minutes. T1: RNase T1 digestion of the substrate RNA. OH: alkaline hydrolysis of the radiolabelled RNA substrate. Asterisk: non-specific product of the reaction. The slightly stronger background degradation detected with GFP-HELZ2 constructs compared to GFP-MBP likely results from co-precipitation of RNA associated with some contaminating activity with the former. (**D**) Quantification of the bands corresponding to the full-length RNA substrate plotted against the time of the reaction in minutes with standard error ($n = 3$).

RNB domain-containing protein, DIS3L1, by performing ribonuclease assays side-by-side. The final products were of comparable size (Supplementary Figure S5) and agree with sizes observed in previous analyses (3). Altogether, these results demonstrate that, despite the presence of a non-canonical residue in its active site, human HELZ2 is an active ribonuclease acting through its RNB domain. Moreover, we did not detect a significant difference in ribonuclease activity between the full-length HELZ2 and the previously described shorter HELZ2β derivative (Figure 3D).

Interestingly, one study recently reported that guanabenz acetate binds HELZ2β with high affinity and activates hepatic leptin receptor expression both *in vitro* and *in vivo*, a property currently under clinical study (42,43). Thus, we tested *in vitro* the degradation of RNA in presence of inhibitory concentrations of guanabenz acetate. We did not observe an effect of this compound on the nuclease activity of HELZ2 (Supplementary Figure S6), suggesting that it may affect other function(s) of the protein.

HELZ2 shows a preference for pyrimidines toward purines nucleotides

Careful examination of the degradation profiles produced by HELZ2 shows that it does not progress uniformly, pausing at certain positions. Matching these points with the RNA sequence indicated that intermediates accumulate when HELZ2 encounters guanosine at the 3′ end of the RNA substrate. To investigate more thoroughly the substrate specificity of HELZ2, we analyzed degradation of hybrid oligonucleotides composed of ten constant 5′ DNA residues followed by twelve 3′ RNA residues either oligo(A), oligo(U), oligo(C) or oligo(G) (The presence of ten DNA residues ensured uniform labeling of the different substrates.). Time-course analysis of the degradation of these substrates using the previously described assay demonstrated a rapid degradation of the oligo(U), less efficient degradation of oligo(C), and limited degradation of oligo(A) (Figure 4A). In contrast, the oligo(G) substrate was barely digested. Comparing the sizes of the final products with the size of a 10 nucleotide long radiolabeled DNA oligonucleotide fractionated in parallel, revealed that HELZ2 degrades the oligo(U) and oligo(C) substrates until only 2–3 ribonucleotides remain on the substrate. This observation suggests tolerance for a DNA backbone in the substrate molecule until a certain point in the path leading to the catalytic center of the protein. Altogether, these data confirm that HELZ2 is unable to degrade DNA substrate and indicate that it has a strong preference for pyrimidine over purine residues for its nuclease activity.

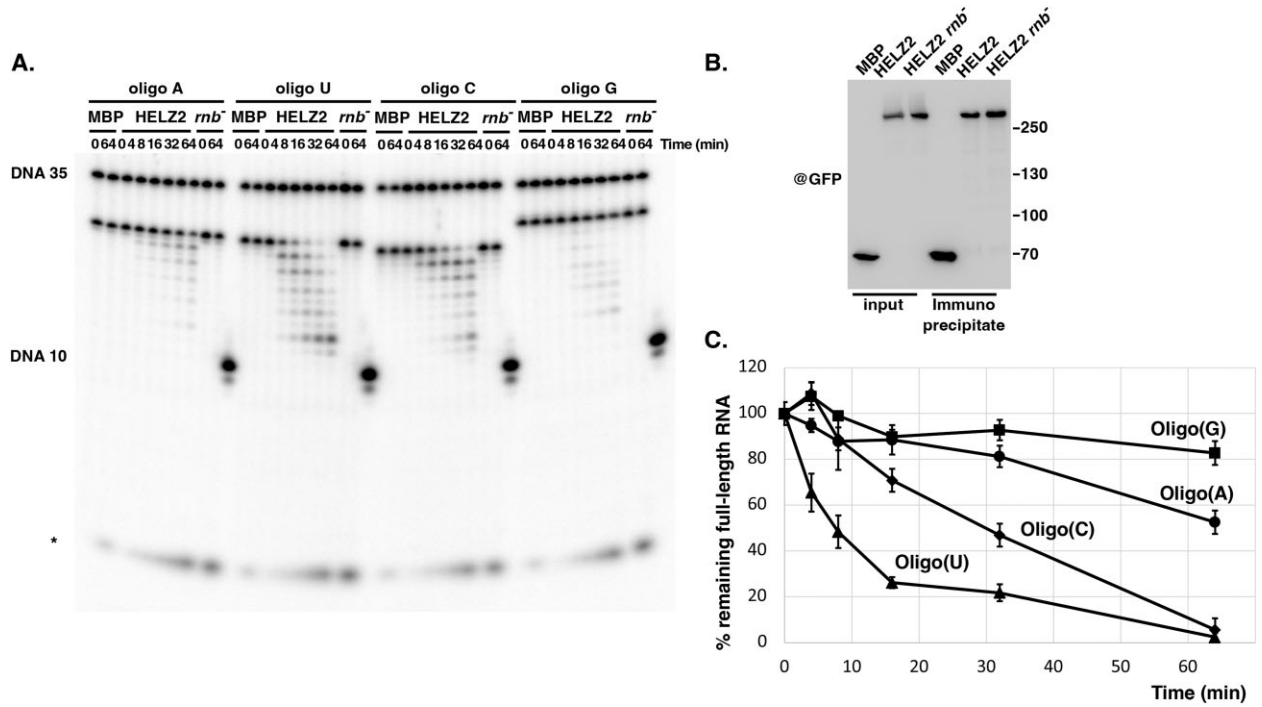

Figure 4. HELZ2 displays substrate preference for pyrimidines. (**A**) Representative RNA degradation assay gel with oligo(A), oligo(U), oligo(C) or oligo(G) containing substrates. Samples from the ribonuclease activity test were fractionated on a 20% polyacrylamide-urea gel. Numbers above the lanes represent incubation times in minutes. A radiolabelled 10 nucleotide long DNA (DNA 10) was also loaded as reference to determine the sizes of the final degradation products. Asterisk: non-specific product of the reaction. (**B**) Western-blot using anti-GFP showing expression levels and immunoprecipitation efficiency for the proteins used in the ribonuclease activity test. (**C**) Quantification of the bands corresponding to the full-length DNA–RNA substrates plotted against the time of the reaction in minutes with standard error ($n = 3$).

HELZ2 exhibits nucleic acid stimulated ATPase activity emanating from its helicase domains

The two helicase domains flanking the RNB domain of HELZ2 contains key amino acids involved in the binding and hydrolysis of ATP. Thus, using the on-bead assay described above, we investigated whether HELZ2 is endowed with ATPase activity. The full-length GFP-HELZ2 protein was used for these reactions with GFP-MBP serving as negative control. We also introduced point mutations of residues required for the binding and hydrolysis of ATP in the motif II of the two helicase domains of HELZ2: DE914/915AA and DE2607/2608AA, to ensure that activities were carried-out by HELZ2. Mutants of individual domains (hel1$^-$ or hel2$^-$), as well as the double mutant (hel1/2$^-$), were constructed. ATPase activity was monitored following incubation with radiolabeled α-P^{32}ATP by monitoring ADP production using Thin Layer Chromatography (TLC) and autoradiography. Incubation of HELZ2 with only ATP resulted in detection of very low ATPase activity after two hours of incubation. Addition of single-stranded nucleic acids, either RNA or DNA, to the reaction significantly increased the production of ADP (Figure 5). As control, incubation of GFP-MBP protein resulted in the production of only background levels of ADP. As DNA was slightly more stimulatory than RNA, we tested whether this did not result from RNA degradation during the assay by testing the activation of the ATPase activity of a RNase defective mutant. DNA remained consistently a marginally better activator, suggesting that this feature is biochemically relevant (Supplementary Figure S7). Testing the role of individual domains using mutant indicated that both domains were active and stimulated by nucleic acids with helicase domain 2 of HELZ2 (hel1$^-$ construct) being more active than helicase domain 1 (Figure 5). Moreover, inactivation of either helicase domain resulted in a more substantial reduction in activity than would be predicted if they acted independently, suggesting a possible coordination of the two helicases. We also investigated the impact of guanabenz acetate on this activity. Again, this compound did not block ATP hydrolysis suggesting that it does not modulate the helicase function of HELZ2 (Supplementary Figure S6).

The HELZ2 nuclease and helicase domains collaborate to degrade structured RNA

The peculiar organization of HELZ2 that includes a unique combination of active helicase domains with a RNB domain may facilitate substrate accessibility to the ribonucleolytic active site. Indeed, members of the RNB family were reported to degrade duplex RNA substrates only as long as it contains a minimal single-stranded 3′ end (4). To test whether HELZ2 can degrade structured RNA, a duplex substrate was produced by annealing a 30 nucleotides RNA with a complementary 14 nucleotides RNA, leaving 16 nucleotides single-stranded as 3′ end (Figure 6). Degradation of this duplex by HELZ2 is stopped after the removal of a maximum of 5 residues. Addition of ATP did not allow the degradation to proceed further (Figure 6). In control

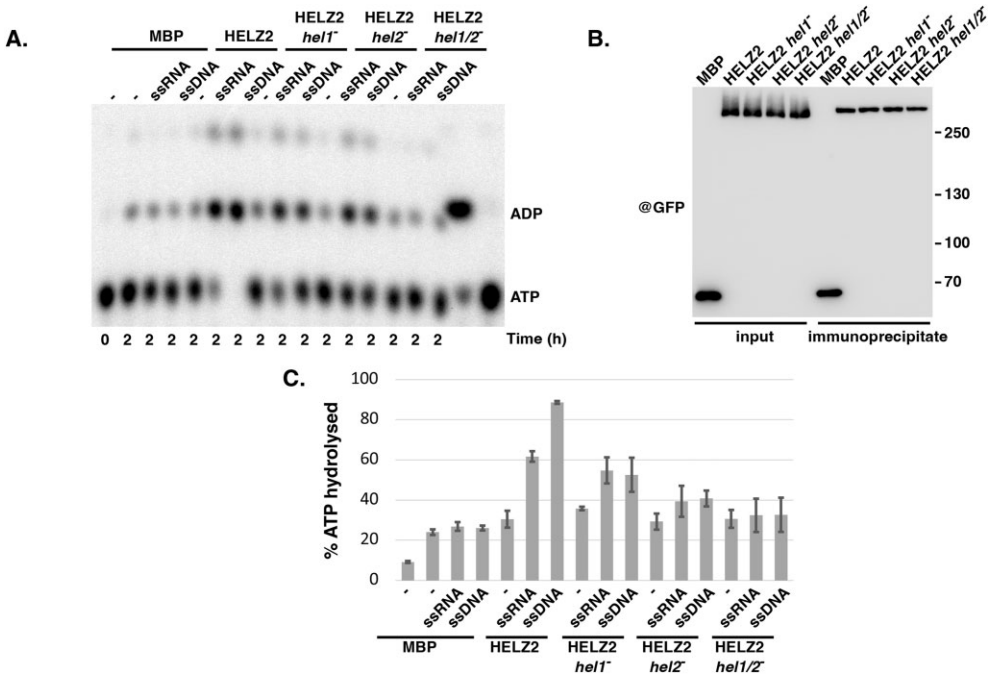

Figure 5. HELZ2 displays nucleic acids stimulated ATPase activity. (**A**) Representative ATPase assay. Samples from the ATPase activity tests were fractionated by thin-layer chromatography (TLC) and detected by autoradiography. Numbers under the lanes represent incubation times in hours. Above the lanes are indicated the nucleic acid substrates used to stimulate ATPase activity and the proteins used for the different assays. The last two lanes are references for the migration of ATP and ADP, respectively. The faint signal at the top represents free phosphate. (**B**) Western-blot using anti-GFP showing expression levels and immunoprecipitation efficiency for the proteins used in the ATPase activity test. (**C**) Quantification of the percentage of hydrolyzed ATP in the various conditions with standard error ($n = 3$).

reactions, the single-stranded 30 nucleotides RNA is efficiently digested, with accumulation of numerous degradation intermediates and the presence of the final 4–5 nucleotide long product (Figure 6). Interestingly, we noticed that addition of ATP stimulated single-stranded RNA degradation. This enhancement was only detected when the helicase domains were active. To test the possibility that a single-stranded entry point is necessary for the unwinding, and thus degradation, of duplex RNA, we designed a substrate incorporating the 14 nucleotide long duplex but in which the complementary strand was prolonged by a 16 nucleotide long single stranded 5′ overhang (Figure 6). This substrate was degraded by HELZ2 beyond the block imposed by the duplex RNA, but only when ATP was present and when the helicase domains were active (Figure 6) Altogether, these results indicate that the helicase domains of HELZ2 collaborate with the RNB domain, giving the protein the ability to degrade structured RNA.

Some mutations found in human diseases abrogate HELZ2 RNase activity

Some patients suffering from primary biliary cholangitis carry the substitution of a threonine by a methionine at position 2151 of the full-length protein (24). Additional genetic alterations of HELZ2 have been identified in cells from cancer patients (44). Interestingly, a somatic D to N substitution at position 1601 of the full-length protein was detected in a patient with melanoma (45). As shown above, this mutation, which alters a critical residue of the HELZ2 catalytic site, blocks its nuclease activity (Figure 3). This observation suggested that other somatic mutations detected in cancer patients may also impact RNA degradation by HELZ2. Thus, we tested the impact of the C1598F, S1920L and R1923L substitutions found in cancer patients (44,46,47), as well as the T2151M mutation, on HELZ2 RNase and DNA-stimulated ATP hydrolysis activities (Figure 7). These mutations had at best modest effect on the ability of the helicase domains to hydrolyze ATP (Figure 7B) but the S1920L and R1923L mutants were unable to degrade RNA (Figure 7B). This is consistent with these substitutions targeting amino acids located next to the substrate RNA in the HELZ2 catalytic center (Supplementary Figure S8, (4)).

DISCUSSION

HELZ2 appears to be an extremely large and complex multifunctional protein. In this study, we have provided evidence that endogenous human HELZ2 is translated from a GUG codon and is thus longer than previously reported. We have also shown that it is an active ribonuclease in spite of the presence of a substitution in the nuclease active site. We also show that the ribonuclease and helicase activities collaborate, allowing the degradation of structured RNAs. This, together with its inducibility by interferon, suggests a role in cellular defense in particular against RNA viruses. HELZ2 is a conserved factor present in many metazoan groups including vertebrates but also invertebrates such as some corals and mollusks. It is, however, absent from some

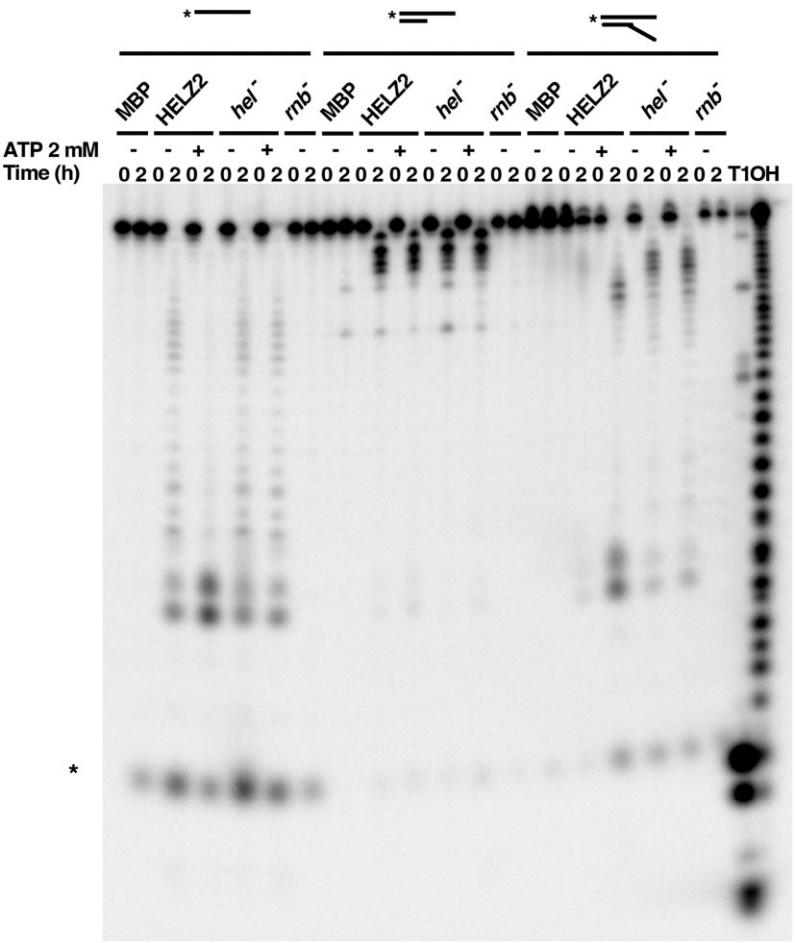

Figure 6. Helicase and ribonuclease activities of HELZ2 synergize for the degradation of structured RNA Representative RNA degradation assay of duplex RNA substrates in presence or absence of ATP. Samples from the ribonuclease activity test were fractionated on a 20% polyacrylamide- urea gel. Numbers above the lanes represent incubation times in hours. Above the figure is a schematic representation of the substrates and proteins used for the assay are indicated. T1: RNase T1 digestion of the substrate. OH: alkaline hydrolysis of the radiolabelled RNA substrate. Asterisk: non-specific product of the reaction.

lineages such as insects, suggesting that it has been lost when organisms encountered conditions in which its function was not advantageous.

The presence of a RNB domain prompted us to analyze the organization and function of the HELZ2 human protein. Careful compilation of available evidences, including transcript mapping data, ribosome profiling results, and comparative genomics suggested that the human HELZ2 protein contained a conserved N-terminal extension not annotated in current databases and that its translation initiates at a non-canonical GUG codon. This possibility was confirmed experimentally. Given this observation, it will be worth reinvestigating whether the previously described HELZ2α and HELZ2β isoforms are also expressed, and if so the biological relevance of the different isoforms. Translation initiation at GUG codon has been reported previously in human cells for viral mRNAs as well as for specific cellular mRNAs such as DAP5/eIF4G2 (48–50). Indeed, transcriptome-wide ribosome profiling experiments (51) and data mining (52) indicate that GUG is, with CUG, the most common substitute to AUG to initiate translation (reviewed in (34)). In this context, it is noteworthy that expression of HELZ2 (PRIC285) in B cells has been shown to be modulated by a polymorphic locus controlling the level of the RPS26 ribosomal protein (28). As RPS26 has been shown to modulate translation initiation by recognizing the Kozak sequence elements upstream of initiation codons and interacts with eIF3 (53,54), it will be of interest to test whether altered RPS26 level modulates HELZ2 translation initiation. Indeed, inefficient initiation at the GUG codon will likely allow recognition of one of the downstream AUG codons, leading to translation of short ORF and probably HELZ2 mRNA degradation by NMD. Taking into account that HELZ2 expression is induced by interferon and that this cytokine has a wide impact on translation (55), future analyses should test whether interferon and/or viral infection can modulate the efficiency of translation initiation at non-AUG codons, particularly in the case of HELZ2.

The presence of a RNB domain in HELZ2 was not reported in the majority of the previous studies mentioning this factor and, consistently, until a very recent study published while this manuscript was in preparation (27), biochemical activity data were lacking. The RNB

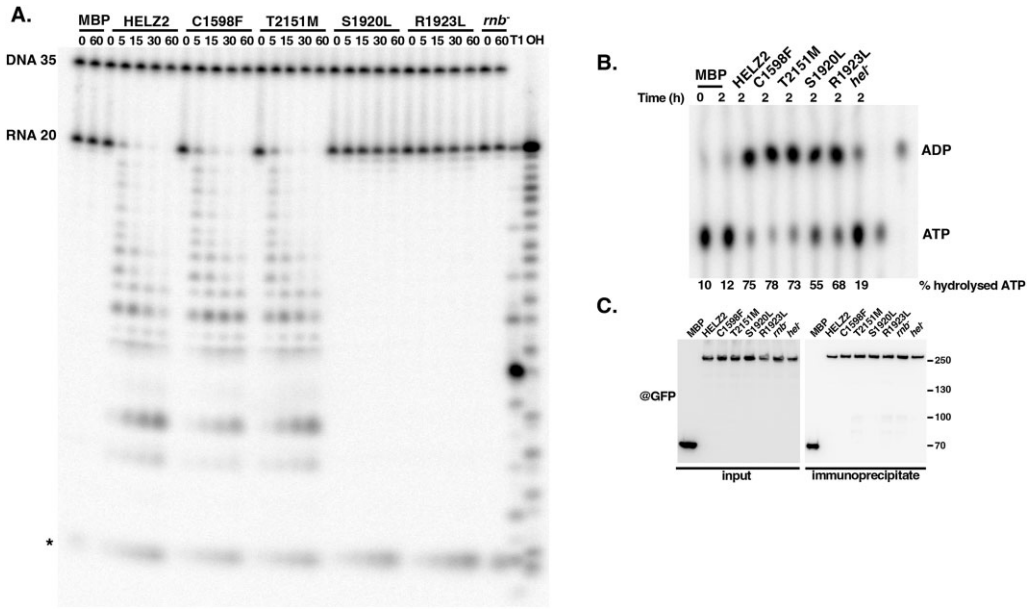

Figure 7. Somatic alterations of HELZ2 inactivate its RNase activity in some cancer patients. (**A**) Representative RNA degradation assay gel from duplicate experiments for the different HELZ2 variants indicated on top. MBP and the rnb- (D1601N) mutant serve as negative controls. Samples from the ribonuclease activity test were fractionated on a 20% polyacrylamide–urea gel. Numbers above the lanes represent incubation times in minutes. T1: RNase T1 digestion of the substrate RNA. OH: alkaline hydrolysis of the radiolabelled RNA substrate. Asterisk: non-specific product of the reaction. (**B**) Representative ATPase assay using the different HELZ2 variants indicated on top. Assays were performed in the presence of DNA to stimulate the ATPase activity. The hel- mutant serves as negative control. Samples from the ATPase activity tests were fractionated by thin-layer chromatography (TLC) and detected by autoradiography. Numbers above the lanes represent incubation times in hours. The fraction of ATP hydrolyzed is indicated below each lane. The last two lanes are references for the migration of ATP and ADP, respectively. (**C**) Western-blot using anti-GFP showing expression levels and immunoprecipitation efficiencies for the proteins used in the ribonuclease and ATPase activity tests.

domain of human HELZ2 contains a substitution of a key aspartate residue in its catalytic center by an asparagine. Yet, our data demonstrate that HELZ2 is an active ribonuclease with characteristics similar to other RNB 3′-5′ exonucleases. The activity of HELZ2 was somewhat unexpected given the conservation of this amino acid in RNB domain-containing proteins. Indeed, this aspartate had been previously proposed to participate in the coordination of catalytic magnesium. However, recent structural analyses reveal that it is involved in interaction with the substrate RNA rather than in the catalytic center (41), a situation that may explain why its substitution with asparagine is compatible with activity. Thus, HELZ2 is the fourth active member of the RNB family in human together with DIS3 and DIS3L1 that are catalytic subunits of the exosome and Dis3L2 a cytoplasmic protein acting on its own to degrade RNA substrates harboring a poly-uridylated 3′ end tail (11,13,56). Like DIS3L2, our data indicate that HELZ2 preferentially degrades substrate ending with U residues. Such substrates are often generated *in vivo* by the action of Terminal Uridyl Transferases (TUTase) adding U to mRNA, small RNA and processing fragments (57). Whether HELZ2 will also target these substrates will have to be determined in the future. Also, the inefficient degradation of poly(A) tail by HELZ2 may suggest that intact endogenous mRNAs may not be the primary targets of this factor. Interestingly, HELZ2 is altered in some autoimmune diseases and as a result of somatic mutations in cancer patients. Three substitutions found in cancer patients (D1601N, S1920L, and R1923L) abolish the HELZ2 RNase activity suggesting that they could contribute to tumor development possibly by weakening the immune system. Other substitutions (C1598F and T2151M) have no discernable effect on HELZ2 RNase activity and all substitutions tested have no discernable effect on HELZ2 ATPase activities. While the C1598F and T2151M may be neutral substitutions, it remains possible that these mutations affect the coordination between the different domains that were not detected in our assays, in particular for the latter that is located between the RNB domain and the final helicase module. Alternatively, these mutations could affect interaction of HELZ2 with partners.

Besides its RNB domain, human HELZ2 contains 6 Zn fingers of two types that may promote binding to single-stranded and double-stranded RNA. Interestingly, highly related Zn fingers are present in the ZC3H7A and ZC3H7B/RoXaN factors (Supplementay Figure 3). Both ZC3H7A and ZC3H7B have been linked to some cancers (58,59). At the molecular level, ZC3H7B/RoXaN was reported to affect miRNA biogenesis by binding specifically to a sequence located in the apical loop of some pri-miRNA. RoXaN also modulates rotavirus infectivity by interacting with the viral non-structural protein 3 (NSP3) that binds the 3′ end of viral RNA. This binding allows the subsequent recruitment of eIF4G to promote their translation at the detriment of endogenous mRNA (60–62). These observations suggest that similarly, the Zn fingers of HELZ2 may interact with RNA. Our current assays with synthetic RNA substrates have not yet provided evidence for the functions of these Zn fingers. Identification of the HELZ2

physiological substrates will certainly provide some clues on their functions.

HELZ2 also contains two helicase domains that are related and belong to the Upf1-like subgroup of the SF1 helicase superfamily. Most members of this subfamily have been shown to interact with RNA and proceed in the 5′ to 3′ direction. Interestingly, the closest relative to the HELZ2 helicase domain 1 and 2 is found in the HELZ protein that has been shown to promote mRNA translation repression and decay (63). Some other members of the Upf1-like subgroup of helicases such as ZNFX1, MOV10 and MOV10L1 interfere with viral infections and/or dispersion of mobile elements (64–66). It is noteworthy that, like HELZ2, ZNFX1 and MOV10 are also interferon-inducible proteins (Figure 2, (67)). Our biochemical data demonstrate that the two helicase domains of HELZ2 are active ATPases stimulated by nucleic acids. Most importantly, they collaborate with the RNB domain, allowing the latter to degrade RNA protected by base-pairing with a complementary RNA (Figure 6), provided that the complementary strand contains a single-stranded 5′-3′ overhang that probably acts as an entry point for one or both helicase domains. Further work will be necessary to understand how the unique combination of domains present in HELZ2 permits the degradation of structured RNA, or possibly RNA-DNA hybrids given that DNA also activates ATPase activities.

Based on the study of knock-out mice, HELZ2 ablation has been described to result in increased leptin receptor mRNA in the liver, leading to reduced lipogenesis and amplified fatty acid oxidation. Mutant mice were resistant to high-fat diet-induced obesity, glucose intolerance, and hepatosteatosis (30). The molecular mechanisms by which HELZ2 affect these processes are not yet deciphered. In particular, while guanabenz acetate has been reported to bind HELZ2 and limit fatty liver and hyperglycemia associated with obesity, we could not observe an effect of this molecule on the RNase and ATPase activities of HELZ2. This suggests the existence of another, yet undefined, function for HELZ2 modulated by guanabenz. The characteristics of HELZ2 including its induction by interferon and nucleic acids, as well as its capacity to degrade structured RNA make it a prime candidate to target viruses and mobile elements that have often compact and structured organization either at the genomic level and/or for their replication intermediates. This is further supported by similarity of regions of HELZ2 with other factors involved in the antiviral response including zinc finger containing proteins (e.g. RoXaN) and RNA helicases (e.g. MOV10). Consistently, HELZ2 was reported to contribute to cellular defense against Dengue virus (21), HCV (22) and Duck Tembusu virus (26). The cytoplasmic localization of HELZ2 would be consistent with some of these activities. More recently, HELZ2 was also reported to inhibit retrotransposition of human LINE1 (27). In contrast, one report suggests that HELZ2 may have a proviral action for SARS-Cov2 (25). However, this statement should be taken with caution given that the CRISPR strategy used in the study may not have taken into account the peculiar non-canonical translation initiation of HELZ2. This issue should be further explored, especially taking into account the reported interaction of HELZ2 with the N protein of SARS-CoV2 (68).

Several ribonucleases acting in response to viral infections are already well characterized (for review, 69). For example, the major OAS/RNase L pathway is activated during viral infection by interferons. Once activated, RNase L will degrade exogenous RNA and ribosomal RNA to block virus production (70–72). RNase L will also degrade cellular mRNA involved in mRNA stability and translation, differentiation and interferon-stimulated genes (72). However, several viruses have developed a way to escape degradation by RNase L (73–76). Understanding the contribution of HELZ2 to the defense against viral infection is thus of great interest in the context of the continuous race between viruses and their host.

DATA AVAILABILITY

All raw LC-MS/MS data have been deposited to the ProteomeXchange via the PRIDE database with (project accession PXD040351). All data is available from the authors upon reasonable request.

SUPPLEMENTARY DATA

Supplementary Data are available at NAR Online.

ACKNOWLEDGEMENTS

We acknowledge members of our team for support and suggestions. We also thank them and Dr P. Reilly for critical reading of the manuscript. We are grateful to Dr. T. Tomaru for the gift of the p3XFLAG-CMV$_{7.1}$ HELZ2β plasmid. Support of IGBMC platforms, particularly the Imaging and Mediaprep facilities, is greatly appreciated.

Authors contributions: Experimental design, E.H. and B.S.; initial experiments J.S.; experiments realization E.H.; mass spectrometry analyses, B.M.; writing of original draft, E.H. and B.S.; manuscript reviewing, E.H., J.S., B.M., B.S.; funding and project supervision, B.S.

FUNDING

Ligue Contre le Cancer (Equipe Labellisée 2020) [to B.S.]; Projet IdEx Exploratoire 2021 [to B.S.]; Interdisciplinary Thematic Institute IMCBio, as part of the ITI 2021–2028 program of the University of Strasbourg, CNRS and Inserm, was supported by IdEx Unistra [ANR-10-IDEX-0002]; SFRI-STRAT'US project [ANR 20-SFRI-0012]; EUR IMCBio [ANR-17-EURE-0023] under the framework of the Plan France 2030. The open access publication charge for this paper has been waived by Oxford University Press – *NAR* Editorial Board members are entitled to one free paper per year in recognition of their work on behalf of the journal.

Conflict of interest statement. None declared.

REFERENCES

1. Arraiano,C.M., Mauxion,F., Viegas,S.C., Matos,R.G. and Séraphin,B. (2013) Intracellular ribonucleases involved in transcript processing and decay: precision tools for RNA. *Biochim. Biophys. Acta - Gene Regul. Mech.*, **1829**, 491–513.

2. Amblar,M. and Arraiano,C.M. (2005) A single mutation in Escherichia coli ribonuclease II inactivates the enzyme without affecting RNA binding. *FEBS J.*, **272**, 363–374.
3. Dziembowski,A., Lorentzen,E., Conti,E. and Séraphin,B. (2007) A single subunit, Dis3, is essentially responsible for yeast exosome core activity. *Nat. Struct. Mol. Biol.*, **14**, 15–22.
4. Lorentzen,E., Basquin,J., Tomecki,R., Dziembowski,A. and Conti,E. (2008) Structure of the active subunit of the yeast exosome core, Rrp44: diverse modes of substrate recruitment in the rnase II nuclease family. *Mol. Cell*, **29**, 717–728.
5. Wasmuth,E.V. and Lima,C.D. (2012) Exo- and endoribonucleolytic activities of yeast cytoplasmic and nuclear RNA exosomes are dependent on the noncatalytic core and central channel. *Mol. Cell*, **48**, 133–144.
6. Schneider,C., Anderson,J.T. and Tollervey,D. (2007) The exosome subunit Rrp44 plays a direct role in RNA substrate recognition. *Mol. Cell*, **27**, 324–331.
7. Mitchell,P., Petfalski,E., Shevchenko,A., Mann,M. and Tollervey,D. (1997) The exosome: a conserved eukaryotic RNA processing complex containing multiple 3′→5′ exoribonucleases. *Cell*, **91**, 457–466.
8. Tomecki,R., Kristiansen,M.S., Lykke-Andersen,S., Chlebowski,A., Larsen,K.M., Szczesny,R.J., Drazkowska,K., Pastula,A., Andersen,J.S., Stepien,P.P. *et al.* (2010) The human core exosome interacts with differentially localized processive rnases: HDIS3 and hDIS3L. *EMBO J.*, **29**, 2342–2357.
9. Staals,R.H.J., Bronkhorst,A.W., Schilders,G., Slomovic,S., Schuster,G., Heck,A.J.R., Raijmakers,R. and Pruijn,G.J.M. (2010) Dis3-like 1: a novel exoribonuclease associated with the human exosome. *EMBO J.*, **29**, 2358–2367.
10. Luan,S., Luo,J., Liu,H. and Li,Z. (2019) Regulation of RNA decay and cellular function by 3′-5′ exoribonuclease DIS3L2. *RNA Biol*, **16**, 160–165.
11. Lubas,M., Damgaard,C.K., Tomecki,R., Cysewski,D., Jensen,T.H. and Dziembowski,A. (2013) Exonuclease hDIS3L2 specifies an exosome-independent 3′-5′ degradation pathway of human cytoplasmic mRNA. *EMBO J.*, **32**, 1855–1868.
12. Ustianenko,D., Hrossova,D., Potesil,D., Chalupnikova,K., Hrazdilova,K., Pachernik,J., Cetkovska,K., Uldrijan,S., Zdrahal,Z. and Vanacova,S. (2013) Mammalian DIS3L2 exoribonuclease targets the uridylated precursors of let-7 miRNAs. *RNA*, **19**, 1632–1638.
13. Malecki,M., Viegas,S.C., Carneiro,T., Golik,P., Dressaire,C., Ferreira,M.G. and Arraiano,C.M. (2013) The exoribonuclease Dis3L2 defines a novel eukaryotic RNA degradation pathway. *EMBO J.*, **32**, 1842–1854.
14. Bayne,R.A., Jayachandran,U., Kasprowicz,A., Bresson,S., Tollervey,D., Wallace,E.W.J. and Cook,A.G. (2022) Yeast Ssd1 is a non-enzymatic member of the rnase II family with an alternative RNA recognition site. *Nucleic Acids Res.*, **50**, 2923.
15. Schoggins,J.W., Wilson,S.J., Panis,M., Murphy,M.Y., Jones,C.T., Bieniasz,P. and Rice,C.M. (2011) A diverse array of gene products are effectors of the type I interferon antiviral response. *Nature*, **472**, 481.
16. Dehler,C.E., Lester,K., Della Pelle,G., Jouneau,L., Houel,A., Collins,C., Dovgan,T., Machat,R., Zou,J., Boudinot,P. *et al.* (2019) Viral resistance and IFN signaling in STAT2 knockout fish cells. *J. Immunol.*, **203**, 465–475.
17. Levraud,J.-P., Jouneau,L., Briolat,V., Laghi,V. and Boudinot,P. (2019) IFN-stimulated genes in zebrafish and humans define an ancient arsenal of antiviral immunity. *J. Immunol.*, **203**, 3361–3373.
18. Xie,X., Liu,P.S. and Percipalle,P. (2019) Analysis of global transcriptome change in mouse embryonic fibroblasts after dsDNA and dsRNA viral mimic stimulation. *Front. Immunol.*, **10**, 836.
19. Yu,S., Mao,H., Jin,M. and Lin,X. (2020) Transcriptomic analysis of the chicken MDA5 response genes. *Genes (Basel)*, **11**, 308.
20. Drouin,A., Wallbillich,N., Theberge,M., Liu,S., Katz,J., Bellovoda,K., Se Yun Cheon,S., Gootkind,F., Bierman,E., Zavras,J. *et al.* (2021) Impact of Zika virus on the human type I interferon osteoimmune response. *Cytokine*, **137**, 155342.
21. Fusco,D.N., Pratt,H., Kandilas,S., Cheon,S.S.Y., Lin,W., Cronkite,D.A., Basavappa,M., Jeffrey,K.L., Anselmo,A., Sadreyev,R. *et al.* (2017) HELZ2 Is an IFN effector mediating suppression of Dengue virus. *Front. Microbiol.*, **8**, 240.
22. Fusco,D.N., Brisac,C., John,S.P., Huang,Y.W., Chin,C.R., Xie,T., Zhao,H., Jilg,N., Zhang,L., Chevaliez,S. *et al.* (2013) A genetic screen identifies interferon-α effector genes required to suppress hepatitis C virus replication. *Gastroenterology*, **144**, 1438–1449.
23. Blanco-Melo,D., Nilsson-Payant,B.E., Liu,W.C., Uhl,S., Hoagland,D., Møller,R., Jordan,T.X., Oishi,K., Panis,M., Sachs,D. *et al.* (2020) Imbalanced host response to SARS-CoV-2 drives development of COVID-19. *Cell*, **181**, 1036–1045.
24. Alexander,M.R., Brice,A.M., van Vuren,P.J., Rootes,C.L., Tribolet,L., Cowled,C., Bean,A.G.D. and Stewart,C.R. (2021) Ribosome-profiling reveals restricted post transcriptional expression of antiviral cytokines and transcription factors during SARS-CoV-2 infection. *Int. J. Mol. Sci.*, **22**, 3392.
25. Biering,S.B., Sarnik,S.A., Wang,E., Zengel,J.R., Leist,S.R., Schäfer,A., Sathyan,V., Hawkins,P., Okuda,K., Tau,C. *et al.* (2022) Genome-wide bidirectional CRISPR screens identify mucins as host factors modulating SARS-CoV-2 infection. *Nat. Genet.*, **54**, 1078–1089.
26. Xiang,C., Yang,Z., Xiong,T., Wang,T., Yang,J., Huang,M., Liu,D. and Chen,R.A. (2022) Construction and transcriptomic study of chicken IFNAR1-knockout cell line reveals the essential roles of cell growth- and apoptosis-related pathways in Duck Tembusu Virus infection. *Viruses*, **14**, 2225.
27. Luqman-Fatah,A., Watanabe,Y., Uno,K., Ishikawa,F., Moran,J.V. and Miyoshi,T. (2023) The interferon stimulated gene-encoded protein HELZ2 inhibits human LINE-1 retrotransposition and LINE-1 RNA-mediated type I interferon induction. *Nat. Commun.*, **14**, 203.
28. Fairfax,B.P., Makino,S., Radhakrishnan,J., Plant,K., Leslie,S., Dilthey,A., Ellis,P., Langford,C., Vannberg,F.O. and Knight,J.C. (2012) Genetics of gene expression in primary immune cells identifies cell type-specific master regulators and roles of HLA alleles. *Nat. Genet.*, **44**, 502–510.
29. Li,P., Lu,G., Wang,L., Cui,Y., Wu,Z., Chen,S., Li,J., Wen,X., Zhang,H., Mu,S. *et al.* (2016) A rare nonsynonymous variant in the lipid metabolic gene HELZ2 related to primary biliary cirrhosis in Chinese Han. *Allergy Asthma. Clin. Immunol.*, **12**, 14.
30. Yoshino,S., Satoh,T., Yamada,M., Hashimoto,K., Tomaru,T., Katano-Toki,A., Kakizaki,S., Okada,S., Shimizu,H., Ozawa,A. *et al.* (2014) Protection against high-fat diet-induced obesity in Helz2-deficient male mice due to enhanced expression of hepatic leptin receptor. *Endocrinol. (United States)*, **155**, 3459–3472.
31. Surapureddi,S., Yu,S., Bu,H., Hashimoto,T., Yeldandi,A.V., Kashireddy,P., Cherkaoui- Malki,M., Qi,C., Zhu,Y.J., Rao,M.S. *et al.* (2002) Identification of a transcriptionally active peroxisome proliferator-activated receptor α-interacting cofactor complex in rat liver and characterization of PRIC285 as a coactivator. *Proc. Natl. Acad. Sci. U.S.A.*, **99**, 11836–11841.
32. Tomaru,T., Satoh,T., Yoshino,S., Ishizuka,T., Hashimoto,K., Monden,T., Yamada,M. and Mori,M. (2006) Isolation and characterization of a transcriptional cofactor and its novel isoform that bind the deoxyribonucleic acid-binding domain of peroxisome proliferator- activated receptor-γ. *Endocrinology*, **147**, 377–388.
33. Abugessaisa,I., Noguchi,S., Hasegawa,A., Kondo,A., Kawaji,H., Carninci,P. and Kasukawa,T. (2019) refTSS: a reference data set for Human and mouse transcription start sites. *J. Mol. Biol.*, **431**, 2407–2422.
34. Kearse,M.G. and Wilusz,J.E. (2017) Non-AUG translation: a new start for protein synthesis in eukaryotes. *Genes Dev.*, **31**, 1717–1731.
35. Michel,A.M., Fox,G., Kiran,A.M., De Bo,C., O'Connor,P.B.F., Heaphy,S.M., Mullan,J.P.A., Donohue,C.A., Higgins,D.G. and Baranov,P.V. (2014) GWIPS-viz: development of a ribo-seq genome browser. *Nucleic Acids Res.*, **42**, D859–D864.
36. Yang,M., Stratford May,W. and Ito,T. (1999) JAZ requires the double-stranded RNA- binding zinc finger motifs for nuclear localization. *J. Biol. Chem.*, **274**, 27399–27406.
37. Kramer,A., Legrain,P., Mulhauser,F., Groöining,K., Brosi,R. and Bilbe,G. (1994) Splicing factor SF3a60 is the mammalian homologue of PRP9 of S.cerevisiae: the conserved zinc finger-like motif is functionally exchangeable in vivo. *Nucleic Acids Res.*, **22**, 5223–5228.
38. Fu,M. and Blackshear,P.J. (2017) RNA-binding proteins in immune regulation: a focus on CCCH zinc finger proteins. *Nat. Rev. Immunol.*, **17**, 130–143.
39. Kanaan,J., Raj,S., Decourty,L., Saveanu,C., Croquette,V. and Le Hir,H. (2018) UPF1-like helicase grip on nucleic acids dictates processivity. *Nat. Commun.*, **9**, 3752.

40. Jumper,J., Evans,R., Pritzel,A., Green,T., Figurnov,M., Ronneberger,O., Tunyasuvunakool,K., Bates,R., Žídek,A., Potapenko,A. *et al.* (2021) Highly accurate protein structure prediction with AlphaFold. *Nature*, **596**, 583–589.
41. Cesaro,G., da Soler,H.T., Guerra-Slompo,E.P., Haouz,A., Legrand,P., Zanchin,N.I.T. and Guimaraes,B.G. (2023) Trypanosoma brucei RRP44: a versatile enzyme for processing structured and non-structured RNA substrates. *Nucleic Acids Res.*, **51**, 380.
42. Yoshino,S., Iwasaki,Y., Matsumoto,S., Satoh,T., Ozawa,A., Yamada,E., Kakizaki,S., Trejo,J.A.O., Uchiyama,Y., Yamada,M. *et al.* (2020) Administration of small-molecule guanabenz acetate attenuates fatty liver and hyperglycemia associated with obesity. *Sci. Rep.*, **10**, 13671.
43. Iwaki,M., Kessoku,T., Tanaka,K., Ozaki,A., Kasai,Y., Yamamoto,A., Takahashi,K., Kobayashi,T., Nogami,A., Honda,Y. *et al.* (2022) Efficacy and safety of guanabenz acetate treatment for non-alcoholic fatty liver disease: a study protocol for a randomised investigator-initiated phase iia study. *BMJ Open*, **12**, e060335.
44. Tate,J.G., Bamford,S., Jubb,H.C., Sondka,Z., Beare,D.M., Bindal,N., Boutselakis,H., Cole,C.G., Creatore,C., Dawson,E. *et al.* (2019) COSMIC: the catalogue of somatic mutations In cancer. *Nucleic Acids Res.*, **47**, D941–D947.
45. Sanborn,J.Z., Chung,J., Purdom,E., Wang,N.J., Kakavand,H., Wilmott,J.S., Butler,T., Thompson,J.F., Mann,G.J., Haydu,L.E. *et al.* (2015) Phylogenetic analyses of melanoma reveal complex patterns of metastatic dissemination. *Proc. Natl. Acad. Sci. U.S.A.*, **112**, 10995–11000.
46. George,J., Lim,J.S., Jang,S.J., Cun,Y., Ozretia,L., Kong,G., Leenders,F., Lu,X., Fernández-Cuesta,L., Bosco,G. *et al.* (2015) Comprehensive genomic profiles of small cell lung cancer. *Nature*, **524**, 47–53.
47. McMillan,E.A., Ryu,M.J., Diep,C.H., Mendiratta,S., Clemenceau,J.R., Vaden,R.M., Kim,J.H., Motoyaji,T., Covington,K.R., Peyton,M. *et al.* (2018) Chemistry-first approach for nomination of personalized treatment in lung cancer. *Cell*, **173**, 864–878.
48. Baril,M. and Brakier-Gingras,L. (2005) Translation of the F protein of hepatitis C virus is initiated at a non-AUG codon in a +1 reading frame relative to the polyprotein. *Nucleic Acids Res.*, **33**, 1474–1486.
49. Kearse,M.G., Goldman,D.H., Choi,J., Nwaezeapu,C., Liang,D., Green,K.M., Goldstrohm,A.C., Todd,P.K., Green,R. and Wilusz,J.E. (2019) Ribosome queuing enables non-AUG translation to be resistant to multiple protein synthesis inhibitors. *Genes Dev.*, **33**, 871–885.
50. Imataka,H., Olsen,H.S. and Sonenberg,N. (1997) A new translational regulator with homology to eukaryotic translation initiation factor 4G. *EMBO J.*, **16**, 817–825.
51. Ingolia,N.T., Lareau,L.F. and Weissman,J.S. (2011) Ribosome profiling of mouse embryonic stem cells reveals the complexity and dynamics of mammalian proteomes. *Cell*, **147**, 789–802.
52. Fedorova,A.D., Kiniry,S.J., Andreev,D.E., Mudge,J.M. and Baranov,P.V. (2022) Thousands of human non-AUG extended proteoforms lack evidence of evolutionary selection among mammals. *Nat. Commun.*, **13**, 7910.
53. Sharifulin,D., Khairulina,Y., Ivanov,A., Meschaninova,M., Ven'Yaminova,A., Graifer,D. and Karpova,G. (2012) A central fragment of ribosomal protein S26 containing the eukaryote-specific motif YxxPKxYxK is a key component of the ribosomal binding site of mRNA region 5′ of the E site codon. *Nucleic Acids Res.*, **40**, 3056–3065.
54. Ferretti,M.B., Ghalei,H., Ward,E.A., Potts,E.L. and Karbstein,K. (2017) Rps26 directs mRNA-specific translation by recognition of Kozak sequence elements. *Nat. Struct. Mol. Biol. 2017 249*, **24**, 700–707.
55. Kroczynska,B., Mehrotra,S., Arslan,A.D., Kaur,S. and Platanias,L.C. (2014) Regulation of interferon-dependent mRNA translation of target genes. *J. Interferon Cytokine Res.*, **34**, 289–296.
56. Chung,C.Z., Jaramillo,J.E., Ellis,M.J., Bour,D.Y.N., Seidl,L.E., Jo,D.H.S., Turk,M.A., Mann,M.R., Bi,Y., Haniford,D.B. *et al.* (2019) RNA surveillance by uridylation- dependent RNA decay in schizosaccharomyces pombe. *Nucleic Acids Res.*, **47**, 3045–3057.
57. Aphasizhev,R., Suematsu,T., Zhang,L. and Aphasizheva,I. (2016) Constructive edge of uridylation-induced RNA degradation. *RNA Biol*, **13**, 1078–1083.
58. Zhou,B., Irwanto,A., Guo,Y.M., Bei,J.X., Wu,Q., Chen,G., Zhang,T.P., Lei,J.J., Feng,Q.S., Chen,L.Z. *et al.* (2012) Exome sequencing and digital PCR analyses reveal novel mutated genes related to the metastasis of pancreatic ductal adenocarcinoma. *Cancer Biol. Ther.*, **13**, 871–879.
59. Astolfi,A., Fiore,M., Melchionda,F., Indio,V., Bertuccio,S.N. and Pession,A. (2019) BCOR involvement in cancer. *Epigenomics*, **11**, 835–855.
60. Vitour,D., Lindenbaum,P., Vende,P., Becker,M.M. and Poncet,D. (2004) RoXaN, a novel cellular protein containing TPR, LD, and zinc finger motifs, forms a ternary complex with eukaryotic initiation factor 4G and rotavirus NSP3. *J. Virol.*, **78**, 3851–3862.
61. Harb,M., Becker,M.M., Vitour,D., Baron,C.H., Vende,P., Brown,S.C., Bolte,S., Arold,S.T. and Poncet,D. (2008) Nuclear localization of cytoplasmic poly(A)-binding protein upon rotavirus infection involves the interaction of NSP3 with eIF4G and RoXaN. *J. Virol.*, **82**, 11283–11293.
62. Treiber,T., Treiber,N., Plessmann,U., Harlander,S., Daiß,J.L., Eichner,N., Lehmann,G., Schall,K., Urlaub,H. and Meister,G. (2017) A compendium of RNA-binding proteins that regulate MicroRNA biogenesis. *Mol. Cell*, **66**, 270–284.
63. Hanet,A., Räsch,F., Weber,R., Ruscica,V., Fauser,M., Raisch,T., Kuzuoglu-Öztürk,D., Chang,C.T., Bhandari,D., Igreja,C. *et al.* (2019) HELZ directly interacts with CCR4- NOT and causes decay of bound mRNAs. *Life Sci. Alliance*, **2**, e201900405.
64. Blasi,G., Bortoletto,E., Gasparotto,M., Filippini,F., Bai,C.M., Rosani,U. and Venier,P. (2022) A glimpse on metazoan ZNFX1 helicases, ancient players of antiviral innate immunity. *Fish Shellfish Immunol.*, **121**, 456–466.
65. Su,F., Liu,X. and Jiang,Y. (2020) Roles of MOV10 in animal RNA virus infection. *Front. Vet. Sci.*, **7**, 569737.
66. Yang,S., Zhang,X., Li,X., Yin,X., Teng,L., Ji,G. and Li,H. (2022) Evolutionary and expression analysis of MOV10 and MOV10L1 reveals their origin, duplication and divergence. *Int. J. Mol. Sci.*, **23**, 7523.
67. Rusinova,I., Forster,S., Yu,S., Kannan,A., Masse,M., Cumming,H., Chapman,R. and Hertzog,P.J. (2013) Interferome v2.0: an updated database of annotated interferon- regulated genes. *Nucleic Acids Res.*, **41**, D1040–D1046.
68. Zheng,X., Sun,Z., Yu,L., Shi,D., Zhu,M., Yao,H. and Li,L. (2021) Interactome analysis of the nucleocapsid protein of SARS-CoV-2 virus. *Pathog. (Basel, Switzerland)*, **10**, 1155.
69. Li,J. and Boix,E. (2021) Host defence rnases as antiviral agents against enveloped single stranded RNA viruses. *Virulence*, **12**, 444–469.
70. Floyd-Smith,G., Slattery,E. and Lengyel,P. (1981) Interferon action: RNA cleavage pattern of a (2′-5′)oligoadenylate–dependent endonuclease. *Science*, **212**, 1030–1032.
71. Silverman,R.H., Skehel,J.J., James,T.C., Wreschner,D.H. and Kerr,I.M. (1983) rRNA cleavage as an index of ppp(A2′p)nA activity in interferon-treated encephalomyocarditis virus-infected cells. *J. Virol.*, **46**, 1051–1055.
72. Brennan-Laun,S.E., Ezelle,H.J., Li,X.L. and Hassel,B.A. (2014) RNase-L control of cellular mRNAs: roles in biologic functions and mechanisms of substrate targeting. *J. Interferon Cytokine Res.*, **34**, 275–288.
73. Min,J.Y. and Krug,R.M. (2006) The primary function of RNA binding by the influenza A virus NS1 protein in infected cells: inhibiting the 2′-5′ oligo (A) synthetase/rnase L pathway. *Proc. Natl. Acad. Sci. U.S.A.*, **103**, 7100–7105.
74. Zhao,L., Jha,B.K., Wu,A., Elliott,R., Ziebuhr,J., Gorbalenya,A.E., Silverman,R.H. and Weiss,S.R. (2012) Antagonism of the interferon-induced OAS-rnase L pathway by Murine coronavirus ns2 protein is required for virus replication and liver pathology. *Cell Host Microbe*, **11**, 607–616.
75. Sorgeloos,F., Jha,B.K., Silverman,R.H. and Michiels,T. (2013) Evasion of antiviral innate immunity by Theiler's virus L* protein through direct inhibition of rnase L. *PLoS Pathog.*, **9**, e1003474.
76. Drappier,M. and Michiels,T. (2015) Inhibition of the OAS/rnase L pathway by viruses. *Curr. Opin. Virol.*, **15**, 19–26.